X-ray spectroscopy of interstellar dust: from the laboratory to the Galaxy

Zeegers, S.T.

5 Interstellar dust scattering of X-rays: the case of AU Microscopii

Abstract

Context The scattering of X-rays by interstellar dust produces halos of diffuse emission around a background source. These halos are used to study the properties of the dust encountered along the line of sight toward the source.

Aims We explore the theory of X-ray scattering for a new parameter space where the small angle approach is no longer valid and where the size distribution of the dust includes large ($> 1\,\mu$m) particles. We apply this theory, for the first time, to the environment of stellar debris disks where such conditions apply. We use as a best test case the debris disk of AU Microscopii (AU Mic).

Methods We make use of the anomalous diffraction theory to calculate the scattering efficiency and the differential scattering cross-section. To model the dust size distribution and dust composition we make use of state of art dust models of the AU Mic debris disk. We construct 40 dust halo models where we vary the stellar wind strength, size distribution and dust composition. These models are compared to a *Chandra* HRC-I observation of AU Mic.

Results A model with a moderate stellar wind strength, a dust size distribution with a steep slope and a dust composition of graphite and astro-silicate would most effectively enhance a dust halo. We find that the size distribution and the stellar wind strength are dominant parameters, whereas the dust composition is of less importance to the halo intensity. From the observational point of view, the theoretical models do not succeed in producing a significant scattering halo, using the current spatial resolution of *Chandra*.

S. T. Zeegers, E. Costantini, F. Paerels, J. Sanz-Forcada, A. G. G. M. Tielens, A. Tiengo

Submitted to A&A

5.1 Introduction

X-ray scattering halos are commonly observed around bright X-ray binaries. These halos arise when the X-rays are scattered by the dust grains along the line of sight. They provide a powerful tool to study the intervening interstellar dust. The possibility of observing such a halo was first proposed by Overbeck (1965). In the last two decades, many X-ray halos have been observed around bright X-ray sources. The earliest observations of X-ray halos were carried out with the *Einstein* (e.g., Mauche and Gorenstein, 1986; Gallagher et al., 1995) and ROSAT satellites (Predehl and Schmitt, 1995). Later studies were carried out using the X-ray telescopes XMM-*Newton* and *Chandra* (e.g Tan and Draine, 2004; Costantini et al., 2005; Smith et al., 2006; Valencic and Smith, 2015). The size and brightness of the X-ray halo depend on the source flux from which the scattered X-rays originate, but also on the particle size distribution, the location of the dust grains along the line of sight, as well as the chemical composition of the dust. In comparison to the source, the halo is faint, containing at most 20% of the soft X-ray emission of the source (Predehl and Schmitt, 1995). Furthermore, the scattering angle is small and forward directed (Overbeck, 1965; Martin, 1970; Hayakawa, 1973), which implies that the dust halo has an arcminute-scale maximum angular size. To observe the halo, it is necessary to use sensitive instruments with a sub arcminute angular resolution, a compact point spread function (PSF) and a low detector background in order to separate the source and the faint halo (Smith and Dwek, 1998). XMM-*Newton* and (especially) *Chandra* provide such an angular resolution. However, determining the dust properties from scattering halos is difficult. The shape of the dust halo depends on both the dust size distribution and the position of the dust along the line of sight, creating a degeneracy between the two effects. When the dust halo is measured at multiple energies it becomes easier to separate the effect of the dust positions from the intrinsic dust properties (Valencic and Smith, 2015). However, the exact position of these clouds, remains difficult to determine. The degeneracy can only be removed in cases of special observing conditions, such as the observation of scattering rings (Vaughan et al., 2004; Tiengo et al., 2010; Heinz et al., 2015; Beardmore et al., 2016; Vasilopoulos and Petropoulou, 2016) or the use of supporting data, e.g., CO-maps (e.g., Smith et al., 2006; Beardmore et al., 2016).

In this study, we apply the theory of scattering halos to an environment which has never been explored before, namely dusty debris disks. As a case study we consider the young, flaring M dwarf star AU Microscopii (Robinson et al., 2001; Hawley et al., 1996). Around this star, a debris disk can be observed (Kalas et al., 2004). This is a circumstellar belt of dust and debris. The sizes of the particles in the disk range from small dust particles up to large unobservable planetesimals (e.g., Lagrange et al., 2000; Wyatt and Dent, 2002). In the youngest stars the dust may be a remnant of the protoplanetary disk, where most of the gas has been expelled from the disk (Wyatt, 2008). This may be the case for AU Mic. However, since the age of the star is estimated to be 23 ± 3 Myr (Mamajek and Bell, 2014), the dust in the debris disk may be the result of constant collisions originating from a so-called birth ring consisting of larger planetesimals (Strubbe and Chiang, 2006). The stellar wind constantly removes the smallest dust particles, which are replenished with dust newly produced by collisions between the planetesimals (Su et al., 2005; Song et al., 2005). Debris disks are interesting objects to study in order to obtain a complete understanding of the dynamics in extrasolar planetary systems. For instance, by studying the properties of the dust in the disk, the composition and

structure of the unseen populations of planetesimals can be investigated (Wyatt, 2008; Krivov, 2010).

The debris disk of AU Mic has been extensively studied at multiple wavelengths from the X-rays (Magee et al., 2003; Mitra-Kraev et al., 2005) and UV (Robinson et al., 2001) to infrared and submillimetre wavelengths (MacGregor et al., 2013). The debris disk can be detected by an infrared excess in the spectral energy distribution (SED) of the star due to the presence of the dust (Tsikoudi, 1988; Song et al., 2002). Since AU Mic is a nearby star, its debris disk can be imaged directly. This has been done at wavelengths from the optical to the near-infrared using the *Hubble Space Telescope* with instruments STIS and ACS (Kalas et al., 2004; Krist et al., 2005) and the Keck II telescope (Metchev et al., 2005), probing dust scattering by submicron sized dust grains. The images revealed a large debris disk, viewed almost perfectly edge-on, which is slightly clumpy in nature and asymmetric. The disk has also been resolved by ALMA (MacGregor et al., 2013). These observations at longer wavelengths show the thermal radiation of larger grains and give an indication of the spatial distribution of these particles. The star itself has been observed in the X-rays several times by different observatories: both XMM-*Newton* and *Chandra* collected images and spectral data of the star. AU Mic is one of the brightest nearby X-ray sources. The X-rays in young M stars, like AU Mic, originate from the corona of the star. This is different from X-ray binaries, where the X-rays originate from the area around a neutron star or black hole, where material from the companion star is falling towards it and is heated to very high temperatures. AU Mic is observed to flare in the UV (Robinson et al., 2001) and X-rays (Mitra-Kraev et al., 2005). These flares may cause short periodical increases in the radiation pressure of the star, which, in that way, causes more and larger particles to be blown out of the disk.

In this chapter, we investigate the possibility of observing the scattered X-ray radiation from the debris disk. In doing so we explore a parameter space which is different from what is common in X-ray halo analysis. This provides us with the possibility to further explore the applications of the halo theory. There are a number of clear differences when we apply the theory to a debris disk compared to X-ray binaries. In contrast to studies of X-ray binaries, we know where the dust is located along the line of sight. In this case, distances towards the star and the disk are well determined. AU Microscopii is part of the β Pictoris moving group and the distance towards the star is 9.94 ± 0.13 pc (Perryman et al., 1997; van Leeuwen, 2007). The debris disk of AU Mic extends at least over 210 AU, based on images at optical wavelength (Kalas et al., 2004; Krist et al., 2005). We are observing dust close to the source in comparison with the total distance to the star, which implies that the scattering halo will be narrow. The dust size distribution deviates from the general ISM, since the smallest particles are blown out of the disk due to the radiation pressure of the star. We base our modeling of the disk on a recent study by Schüppler et al. (2015) and Augereau and Beust (2006) (hereafter S15 and AB06, respectively), taking into account the composition and structure of the dust grains, the size distribution of the grains and stellar activity. In our analysis of the debris disk we make use of observations from *Chandra*.

The chapter is structured as follows: in Section 5.2 we describe the halo theory under the geometrical conditions of a debris disk. In Section 5.3 we show the observation of the debris disk with *Chandra*. In Section 5.5 we discuss the results of the fits to the dust halo of AU Mic and in Section 5.6 we give our conclusions.

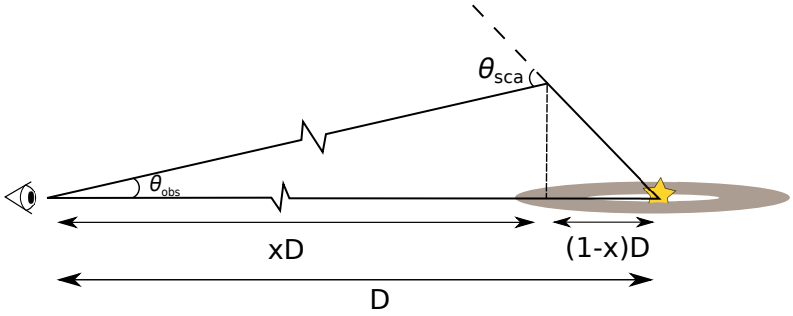

Figure 5.1: Geometry of X-ray scattering in the debris disk of AU Mic. The total distance to the source, given by D, is 9.93 pc. The dust is situated in the debris disk which extends over 210 AU. The distance from the dust to the source is indicated by (1-x)D and the distance from the observer to the dust is given by xD. The scattering angle is indicated by $\theta_{\rm sca}$ and $\theta_{\rm obs}$ indicated the angle at which the scattered X-rays are observed.

5.2 X-ray dust models for debris disk: the halo model

The scattering intensity of the scattering halo can be obtained using the general equation (Mathis and Lee, 1991):

$$\begin{aligned} \mathrm{I}(\theta_{\rm obs}) = N_{\rm H} \int_{\rm E_{min}}^{\rm E_{max}} S(E)dE \times \int_{\rm a_{min}}^{\rm a_{max}} n(a)da \\ \times \int_0^1 \frac{f(x)\cos(\theta_{\rm sca}-\theta_{\rm obs})}{(1-x)^2} \frac{d\sigma(a,E,\theta_{\rm sca},x)}{d\Omega} dx, \end{aligned} \tag{5.1}$$

where $\mathrm{I}(\theta_{\rm obs})$ is the intensity of the halo at a certain observed angle from the source. The integration is computed over the energy given by E, particle size given by a and the fractional distance to the source given by x, where $x = 0$ at the observer and $x = 1$ at the source. $N_{\rm H}$ is the hydrogen column density towards the source. $S(E)$ is the spectral energy distribution of the source. The function $f(x)$ is the density of hydrogen at a distance xD, relative to the average density on the line of sight toward the X-ray source (Mathis and Lee, 1991). D is the total distance to the source. $n(a)$ is the particle size distribution. The differential scattering cross-section $\frac{d\sigma}{d\Omega}$ is a function of a, E, and $\theta_{\rm sca}$.

Since the particle size distributions used in this analysis contain large particles ($> 1\,\mu$m), we make use of the Anomalous Diffraction Theory (ADT) to calculate $\frac{d\sigma}{d\Omega}$. The Rayleigh-Gans approximation only holds for smaller grains (Hoffman and Draine, 2016). Furthermore, Mie theory cannot be used due to round-off errors that arise for values of the size parameter ($X = \frac{2\pi a}{\lambda}$) larger than 10^4 (Hoffman and Draine, 2016). We use the ADT code adt.f[1] to calculate $\frac{d\sigma}{d\Omega}$.

In the case of AU Mic, the vertical optical depth does not exceed $\tau = 5 \times 10^{-3}$, which indicates that the disk in optically thin (AB06). In Figure 5.1 we describe the geometry of the

[1]available at: www.astro.princeton.edu/~draine/scattering.html

system. Here, it can be seen that the dust is situated relatively close to the source in comparison with the total distance towards AU Mic. Therefore, we cannot use the commonly applied small angle approximation between the observed angle, $\theta_{\rm obs}$, and the scattering angle, $\theta_{\rm sca}$, but we use the formal relation (e.g., Smith et al., 2016):

$$\theta_{\rm sca} = \arctan\left(\frac{x\tan(\theta_{\rm obs})}{1-x}\right) \tag{5.2}$$

$f(x)$ can be expressed as:

$$f(x) = \frac{n_{\rm H}(x)\mathrm{D}}{N_{\rm H}}, \tag{5.3}$$

where $n_{\rm H}(x)$ is the number density of hydrogen particles (Smith and Dwek, 1998). If the dust were smoothly distributed along the line of sight $f(x) = 1$. The total column density of hydrogen measured in the X-rays consist of both atomic and molecular hydrogen. The atomic hydrogen traces mostly the contribution of the ISM, whereas molecular hydrogen traces the circumstellar stellar matter. A value of $N_{\rm H} = 1 \times 10^{18}\,{\rm cm}^{-2}$ for the contribution of the ISM has been found by Monsignori Fossi et al. (1996) using a calculation based on other stars and by Wood et al. (2005) using H I L$y\alpha$ emission lines. The ISM absorption can also be calculated directly using the EUV line flux ratio of the Fe XVI doublet at 335 and 360 Å lines, following Sanz-Forcada et al. (2003, and references therein), resulting in a value of $N_{\rm H} = 1 \times 10^{18}\,{\rm cm}^{-2}$. The disk around AU Mic contains molecular hydrogen. This is accounts for the majority of the hydrogen along the line of sight. The value, however, has a large uncertainty. Following the discussion in Schneider and Schmitt (2010) we assume a value of $N_{\rm H} < 1 \times 10^{19}\,{\rm cm}^{-2}$ as an upper limit for the total hydrogen column density. In this analysis of the AU Mic debris disk we assume, as a first approach, that the contribution of the ISM to the column density is negligible and that the density within the disk is constant. The integration over x in Equation 5.1 can then be performed solely over the disk. With these assumptions Equation 5.3 is now simplified to:

$$f = \frac{\mathrm{D}}{R_{\rm disk}}, \tag{5.4}$$

where D is the total distance (i.e. from the observer to the star) and $R_{\rm disk}$ is the radius the debris disk.

5.2.1 Particle size distribution

The size distribution of particles within a debris disk of the type of AU Mic is determined by the collisions in the disk. The dust is thought to originate from a so-called birth ring of larger colliding bodies that act as a dust particle reservoir. After a certain dynamical time the disk will reach a collisional equilibrium state (Backman and Paresce, 1993; Augereau and Beust, 2006).

The size distribution can be expressed as:

$$n(a)da = K_i a^{-q} da \tag{5.5}$$

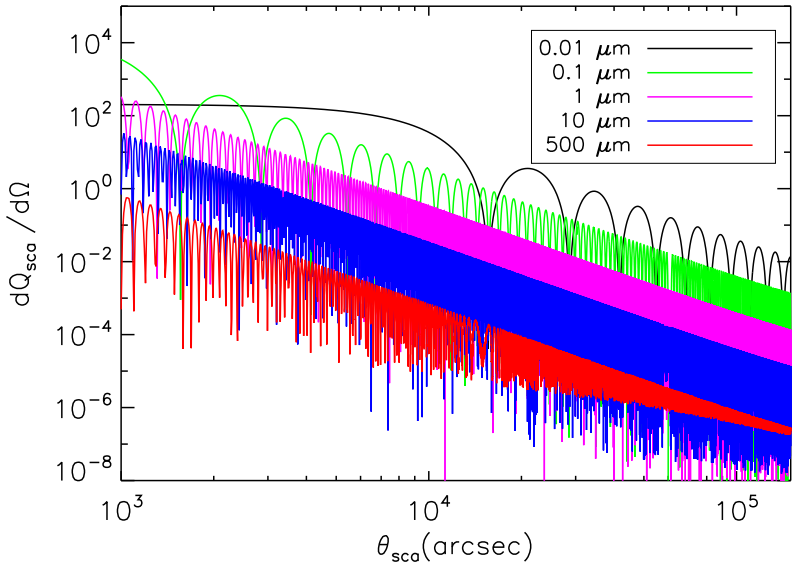

Figure 5.2: The differential scattering efficiency versus the scattering angle for several particle sizes, up to 500 micron. The calculations were done using the adt.f code.

The value of q determines the slope of the size distribution. The larger the absolute value, the steeper the distribution becomes. A value of $q = 3.5$ would hold for systems in collisional equilibrium (Dohnanyi, 1969).

However, the slope of the dust size distribution of debris disks can deviate from the classical value valid for a collisional equilibrium (Durda and Dermott, 1997; Wyatt and Dent, 2002). The disk can often be modeled using values of q larger than 3.5. In the case of AU Mic, there are different possible values of the slope. In our modeling, we include both a flatter and steeper distribution than the typical one. We use 3.3, 3.5, 3.8 and 4.1 (S15; AB06).

The parameter K_i takes care of the normalisation of the size distribution for a certain dust composition i. The value of the normalisation is different depending on the chemical composition of the dust and the dust size distribution. For the derivation of K_i we follow the method of Mauche and Gorenstein (1986):

$$\int \sigma_{\rm sca}(a) a^{-q} n(a) {\rm d}a = n_g \sigma_{\rm sca}, \tag{5.6}$$

with $n_g \sigma_{\rm sca} = 0.18\,{\rm kpc}^{-1}$ at 1 keV for standard grain parameters (Mauche and Gorenstein, 1986) of interstellar dust. We use ADT to calculate $Q_{\rm sca}$, from which we obtain $\sigma_{\rm sca} = Q_{\rm sca}\pi a^2$ and apply a numerical integration over the dust distribution models relevant for AU Mic.

The size of the smallest particles in the disk depends on the stellar wind strength and the stellar radiation pressure of the star. The radiation pressure can remove the smallest particles from the disk. The opposite effect is the Poynting-Robertson drag, which can be ignored,

Table 5.1: Models of the AU Mic debris disk

Model	Composition	B.S. (μm) SW50	B.S. (μm) SW300	optical constants (n, $k \times 10^{-5}$)
M1	sil33+car33+vac33	0.07	0.48	(0.81, 4.19)
M2	sil50+car50	0.04	0.35	(0.99, 5.16)
M3	sil25+car25+ice25+vac25	0.07	0.51	(0.87, 4.05)
M4	sil10+car10+ice40+vac40	0.11	0.71	(0.77, 3.25)
M5	sil15+car15+vac70	0.16	0.93	(0.55, 2.82)

Models used to describe the composition of the dust in the debris disk AU Mic following the modeling of S15. The first column indicates the names of the five different dust mixture models. The second column describes the content of the dust mixtures, where for example sil25+car25+ice25+vac25 stands for volume fractions of 25% astrosilicate, 25% graphite, 25% water ice and 25% vacuum to indicate the level of porosity. The third and the fourth column show the minimum size a dust grain in the disk can have, smaller particles are blown out of the disk due to the stellar wind. The third column indicates the minimum grain sizes (i.e., the blowout size, B.S.) for moderate stellar wind strength (SW50) and the fourth column indicates the minimum grain sizes for strong stellar wind strength. The fifth column shows the optical constants n and k for each dust mixture at 1 keV.

since the time scale, on which P-R drag would become important is very long, which means that the debris disk would become so low in density that it is no longer detectable with current instrumentation (Wyatt, 2005, AB06).

The total stellar wind force acts upon the particles in a similar way as the radiation pressure: the particles can either be blown from the disk, due to the stellar wind pressure, or dragged towards the star, due to a loss of angular momentum created by the stellar wind, which acts as headwind on the particles (Burns et al., 1979). The latter effect is referred to as stellar wind drag. If the stellar wind is strong, which it is in the case of young flaring M stars such as AU Mic, the effect of the stellar wind drag on the dust particles in the disk is small. The stellar wind pressure does in fact effectively remove the smallest particles from the disk. The particles are either expelled from the disk or end up in the outer parts of the disk. The stronger the stellar wind, the larger the particles that are blown out of the disk.

The minimum size that a particle in the disk can have is referred to as the blowout size. The stellar wind strength is expressed in multiples of the solar mass loss rate ($\dot{M}_\odot = 2 \times 10^{-14}\, M_\odot \mathrm{yr}^{-1}$). Following the modeling of S15 and AB06, we use two different stellar wind strengths (SW): SW50 representing a moderately strong stellar wind i.e. $\dot{M}_\star = 50\dot{M}_\odot$ and SW300, representing 300 times the solar wind strength ($\dot{M}_\star = 300\dot{M}_\odot$). In the case of the SW50 model, flares are ignored (S15;AB06), while the SW300 model averages over the flare and quiescent phases (S15). The high wind strength causes the stellar wind pressure to be greater than the radiation pressure (S15). Here, we will not consider a model where there is no stellar wind activity, since modeling of AU Mic system shows a strong preference for a model including stellar wind activity, which is supported by the frequently observed flares in AU Mic (Cully et al., 1993). The largest particles in the size distribution have a modest influence on the total scattering, since they are less represented due to the slope of the size distribution. In this analysis, we will include particle sizes up to 1 mm (see Figure 5.3) and assume spherical particles.

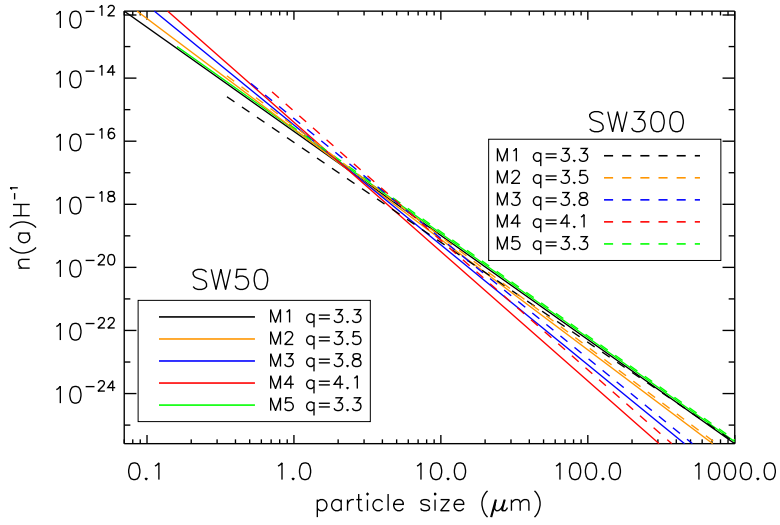

Figure 5.3: The particle size distribution for a subset of dust models used in this analysis. The models differ in slopes and size range and for each of these we selected the dust compositions as indicated in Table 5.1. The dashed set of models show the size distribution of the strong stellar wind model (SW300) and the colors indicate the different slopes for which we chose one dust mixture as an example. The slope q=3.3 is repeated to also show the M5 dust mixture. In the same way, we show the models for the moderately strong stellar wind model (SW50).

5.2.2 Scattering efficiency versus energy and particle size

The scattering efficiency of a particle changes for different particle sizes and at different energy (Figure 5.4). We use the optical constants of an astro-silicate (Draine and Lee, 1984; Laor and Draine, 1993). The strength of the scattering efficiency, $Q_{\rm sca}$, is indicated by the color bar. At certain values of the energy and particle size, scattering is more efficient. At 1 keV, for example, the most efficient scatterers have sizes between 0.4 and 1 μm. As the energy increases the particle size of the efficient scatterers also increases. However, at certain energy values the efficiency drops abruptly. This is due to the absorption edges of respectively oxygen, iron (L-edge), magnesium and silicon, as indicated in Figure 5.4. At the edge an X-ray photon is more likely to be absorbed, because it has an energy just above the binding energy of the electron. At slightly higher energies close to the edge $Q_{\rm sca}$ increases and decreases, these feature are the X-ray Absorption Fine Structures (XAFS). The XAFS arises when a X-ray photon excites a core electron, which in turn causes an outwardly propagating photo-electron wave. The wave is scattered by the neighboring atoms from which new waves will emanate. These waves are superimposed on the wave function of the photo-electron, causing constructive and destructive interference near the edge. This effect propagates in the optical constants, which in turn influences the absorption and scattering efficiencies. At energies near the edge $Q_{\rm sca}$ can change rapidly. As the particle size increases beyond 1 μm, $Q_{\rm sca}$ stabilizes to a value

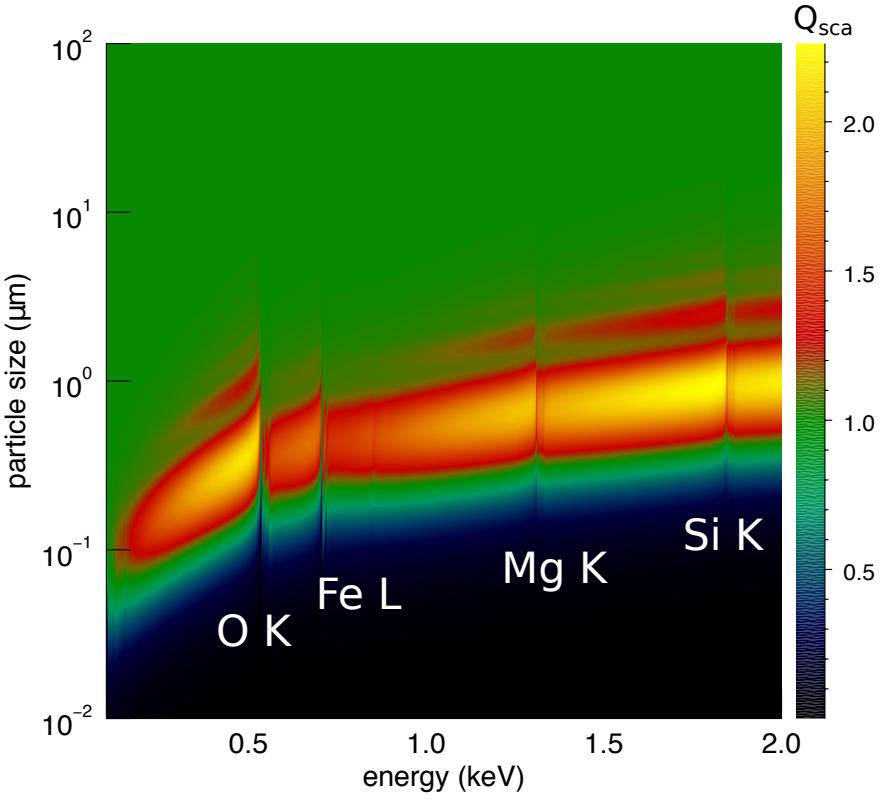

Figure 5.4: Scattering efficiency, indicated by the colorbar, as a function of the Energy in keV versus the particles size in μm for an astro-silicate. The positions of the oxygen K-edge, iron L-edge, magnesium K-edge and silicon K-edge are indicated in the figure.

of 1, which is expected in the geometrical regime where the wavelength is small compared to the particle size.

5.2.3 Dust mixtures in debris disks

Although the planetesimals, from which the dust in the debris disk originate, cannot be directly detected, the dust in the debris disk can help in revealing the composition of these planetesimals. They are often compared to Kuiper belt objects and the dust in debris disks may thus resemble the chemical composition and porous structure of comets in the Solar system (Wyatt, 2008; A'Hearn et al., 2005).

The chemical composition of dust in debris disks can be probed by studying distinctive features in the mid- and far-infrared spectra of the disks. Several disks were well matched with a mixture of amorphous and crystalline silicates and carbonaceous material (i.e. HD

69830, Beichman et al. (2005); Lisse et al. (2007), HD 172555, Lisse et al. (2009), β Pictoris, de Vries et al. (2012), Fomalhaut, Lebreton et al. (2013)). In some cases also water ice was detected (i.e. HD 181327, Chen et al. (2008); Lebreton et al. (2012)). The debris disk of AU Mic in particular is best modeled using porous grains containing a heterogeneous mixture of silicate, graphite and ice (Graham et al., 2007; Fitzgerald et al., 2007). Therefore, we use the optical constants of graphite, astro-silicate (Draine, 2003) and water ice in our analysis to calculate the optical constants of the dust mixtures. In the case of water ice, we took the optical constants of water from the CXRO X-ray database (Henke et al., 1993) with a density of 0.9167 g/cm^3. In Table 5.1 we indicate the different mixtures that we used in the analysis, here we follow the analysis and nomenclature in Schuppler et al. 2015. Five different dust mixtures are used with different contributions of silicates (sil), graphite (car) and water ice (ice). We test several levels of porosity, indicated by the percentages of vacuum (vac) in the grains. The first column in Table 5.1 indicated the number of the model. The second column gives the composition, where the corresponding number indicated the volume fraction of the material in percentages. In the fourth column, the blowout sizes are given per dust mixture and stellar wind model (S15). We also give the optical constants (n and k) for the dust mixtures at 1 keV in the fifth column. The optical constants of the composite dust particles are generally obtained using a mixing rule (also referred to as the effective optical constants). S15 use the Bruggeman mixing rules (Bruggeman, 1935), which cannot be applied in our case, since the particles are large compared to the wavelength. Different mixing rules predict different values of the optical constants, but they are bound by a maximum value, so called Wiener bounds (Wiener, 1910). We approach the value of the effective optical constants by the maximum value ($\epsilon_{\mathrm{eff,max}}$) they would have in the following way:

$$\epsilon_{\mathrm{eff,max}} = \sum f_i \epsilon_i, f_i = \frac{V_i}{V_{\mathrm{total}}}. \tag{5.7}$$

Here f_i is the volume fraction of the ith component of the mixture and ϵ_i is the permittivity. The optical constants n and k can be derived from $\epsilon_{\mathrm{eff,max}}$.

5.3 X-ray scattering by dust in the AU Mic debris disk

AU Microscopii was observed three times by *Chandra* and both spectral and imaging data are available. In the first two observations, with obsid 17 and 8894, gratings were used in order to obtain stellar spectra. The images from these observations cannot be used in this analysis, since the presence of a grating affects the radial profile, which we want to extract. Therefore, we use image data taken by the High Resolution Camera (HRC) (Murray et al., 2000). One of the two detectors, the HRC-I detector, of this instrument is optimized for imaging. The HRC has an energy range from 0.06-10 keV albeit without energy resolution of the source. AU Mic was observed on the 17th of August 2010 (obsid 12236) for a duration of 23.9 ks. The HRC detector is most efficient at 1.5 keV[2]. The source is expected to be bright around 0.5-1 keV (Magee et al., 2003). Our models will therefore be tested at 1 keV.

The data needed some processing in addition to the standard pipeline. In particular, the event image showed a jet-like ghost. This is a well-known artefact which originates in the

[2]http://cxc.harvard.edu/csc/columns/ebands.html

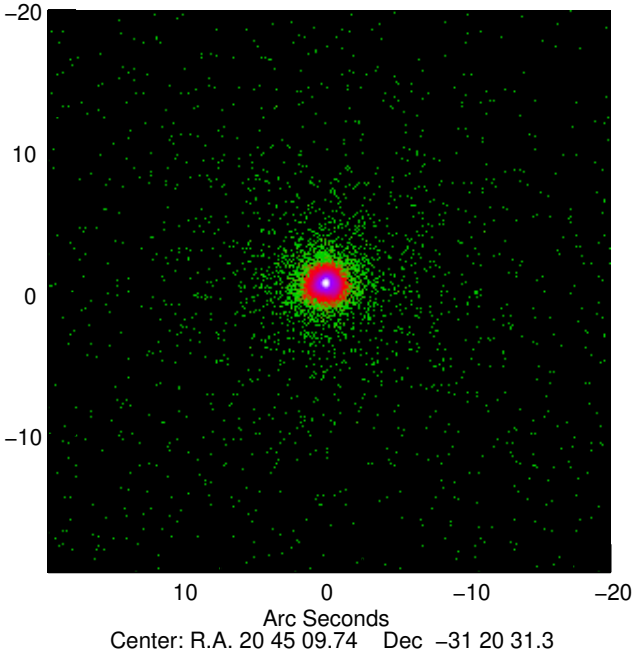

Figure 5.5: *Chandra* HRC-I observation of AU Mic (obsid 12236) after the application of additional processing in order to remove a jet-like ghost feature.

HRC-I detector (Murray et al., 2000). The ghost is usually reduced to $< 0.1\%$ of the total flux by standard processing. In the case of the observation of AU Mic, the jet was still present in the reduced images. A solution to this problem is to filter out these events by ignoring the third amplifier. This decreases the flux slightly, but since we are interested in the morphology of the halo, the slight reduction in the overall brightness of the source does not affect our analysis. The final image can be seen in Figure 5.5.

We extracted the surface brightness profile using 23 logarithmically spaced annuli for the spatial analysis of the halo. This was done using the standard CIAO software[3]. We evaluate the halo up to 30 arcsec away from the source. We conservatively assume a circular geometry around the source, since we do not have any imaging information on the geometry of the disk in the X-rays. Obervations at different wavelength have indeed revealed different disk geometries (e.g., HST (Kalas et al., 2004), ALMA (MacGregor et al., 2013)), tracing different dust particle sizes. The X-rays may reveal a geometry which is slightly different from what is observed at longer wavelengths, since the X-rays are sensitive to the very small submicron dust particles, as can be seen in Figure 4. These small dust particles can be pushed into eccentric or unbound trajectories due to the stellar wind interacting with the disk and may, in this way, end up slightly out of the plane of the disk (Boccaletti et al., 2015).

[3]http://cxc.harvard.edu/ciao/threads/radial_profile/

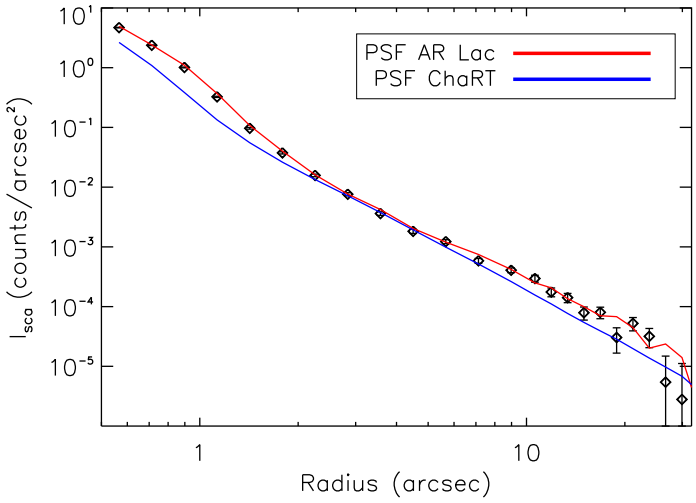

Figure 5.6: This figure shows the radial profile, halo intensity versus radius in arcsec, of the observation of AU Mic, indicated by the diamond symbols. The blue line shows the PSF obtained using ChaRT and the red line shows the radial profile of the star AR-Lac which is used as a PSF in this chapter.

The PSF of the image was first obtained using the *Chandra* ray tracing software: ChaRT (Carter et al., 2003) and using CALDB and CIAO with version 4.7.3 and 4.9 respectively. The PSF obtained by ChaRT and the in-flight PSF are known to deviate. At small angles this is caused by an asymmetry in the PSF of *Chandra*, which becomes apparent when the image is deconvolved with the PSF. The asymmetry has a hook-like structure and occurs in the images at ~ 0.6 – 0.8 arcsec and changes over the long time scales. This feature appeared between October 1999 and December 2000 and was first observed in the calibration data of the star AR Lacertae (AR Lac). Over time this star has been regularly observed in order to monitor the asymmetry. Therefore, we used AR Lac as a point like source. This is an unresolved spectroscopic binary star. This system has no known disk and can therefore be used as a PSF calibrator. In this way, we can compare the PSF obtained by ChaRT. We use an observation of 20 ks from the 16th of December 2010 (obsid 13182), close in time to the observation of AU Mic. In Figure 5.6 we show the radial brightness profile of both AR Lac and AU Mic compared to the ChaRT-PSF. As can be seen, the radial profile of AR Lac closely follows that of AU Mic at both small angles (< 1 arcsec) and angles >10 arcsec.

5.4 The halo modeling

We constructed the halo models using the five different dust compositions listed in Table 5.1, four different values of the size distribution, as well as two different values of the stellar wind strength. This resulted in 40 halo models. The dust halo intensity was derived using equation 5.1, where we used ADT to calculate the $d\sigma/d\Omega$ and the energy is fixed to 1 keV (see

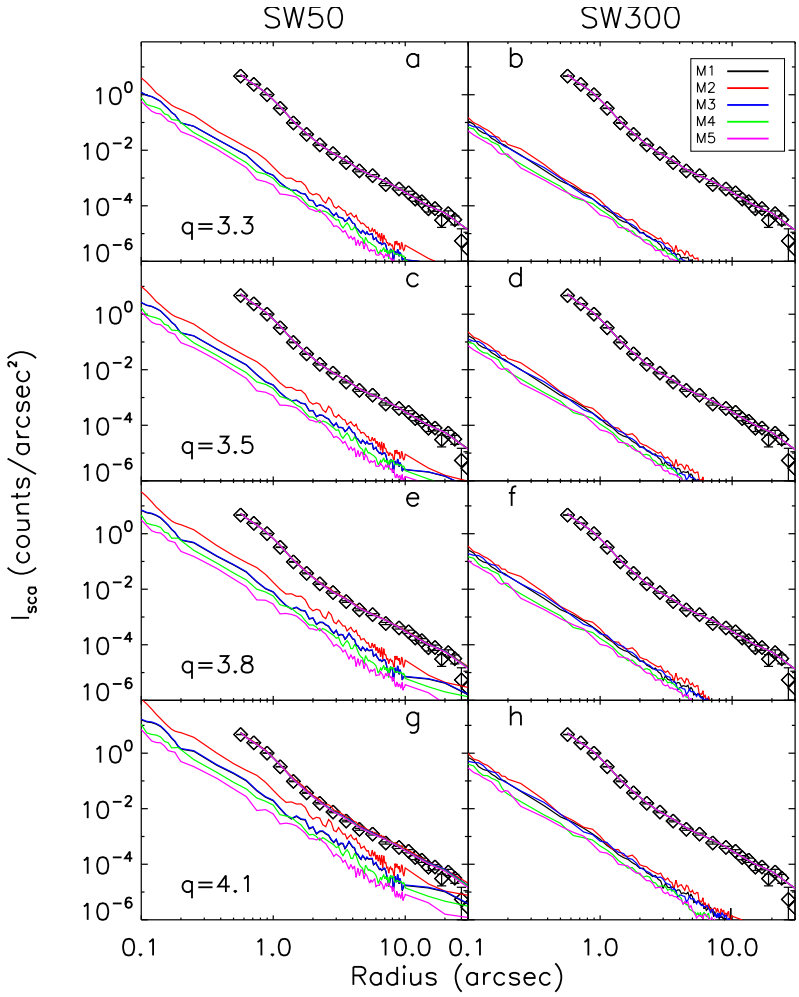

Figure 5.7: This figure contains all the models considered in this analysis, forty models in total. The two columns show the different stellar wind activity. Each row indicates a different value of the slope of the size distribution q. The colors in each panel indicated the different dust mixture models (M1, M2, M3, M4 and M5) used in this analysis. The contribution of the scattering dust to the radial profile, where the PSF is subtracted, is shown by the lines below the observed profile. In this way, the differences between dust mixtures can be observed more easily. The models are also shown in the case where the PSF is included. In almost all the models, the contribution of the scattered dust is so small, that the models fall on top of each other. The diamond symbols indicate the data points of the radial profile of AU Mic.

Section 5.2.3). These models are compared with the observation of AU Mic in Figure 5.7. The halo models are evaluated from 0.1 arcsec up to 30 arcsec. The small angles (0.1-0.5 arcsec) are included to show the behaviour of the models for angles that are inaccessible for *Chandra*. The plots on the left-hand side show the results for the low stellar wind strength (SW50) and the column on the right-hand side the high stellar wind strength (SW300). The rows indicate the different values of the slope of the dust size distribution. The diamond symbols indicate the data points of the radial profile of AU Mic. The halo has been modeled out to a radial distance of 30 arcsec. Beyond 30 arcsec the intensity of the source drops and our models do not show any significant contribution of the halo. Beyond 10 arcsec we used a coarser spacing of the data points, since the calculations for angles larger than this value become time consuming. When the slope of the size distribution becomes steeper, the amount of small particles increases. These particles are the effective scatterers (Figure 5.4). This effect is particularly visible in the left column, because if the stellar wind is strong (SW300), most of the small (<1 μm) particles are blown out of the disk. This means that the most effective scatterers are now removed from the model, whereas they are still present in the moderately strong stellar wind model (SW50). The five dust mixtures (M1, M2, M3, M4 and M5) are represented in Figure 5.7 by different colors. The contribution of the scattering dust to the radial profile, where the PSF is subtracted, is shown by the lines below the observed profile. In this way, the differences between dust mixtures can be observed more easily. The models are also shown in the case where the PSF is included. For most of the models the halo contribution is very low and therefore the dust mixture models in almost all of the frames fall on top of each other. The models in panel *g* have the highest impact on the scattering halo. These models have the steepest size distribution (q=4.1) and a moderate stellar wind strength (SW50). The dust mixture that contributes the most to the scattering halo is the M2 dust mixture, which contains volume fractions of 50% astro-silicate and 50% graphite.

5.5 Discussion

In this chapter, we explore a new parameter space, which is different from the parameter space addressed in studies of X-ray halos of X-ray binaries. In this new parameter space the small angle approximation is no longer valid (see Section 5.2.1). Moreover, we address a broader size distribution, where we include large particles with sizes up to 1 mm as prescribed by studies on debris disks. The smallest particles in the size distributions of our models are still considered large when compared to the Mathis-Rumpl-Nordsieck (MRN, Mathis et al. (1977)) size distribution which is commonly used when studying dust in the ISM. The smallest particles in the MRN distribution have a size of 0.005 μm in comparison to the smallest particles in our models of 0.04 μm.

We applied the scattering theory to the nearest edge-on debris disk, AU Mic. Here we make use of the state of the art dust models based on the modeling of this disk in scattered light (S15;AB06). The parameters of the dust models that affect the dust halo are the slope of the size distribution, the composition of the dust, the stellar wind activity and the value of $N_{\rm H}$.

The halo is of course also affected by the brightness of the source itself. AU Mic is a unique source in this type of study, since it is a very bright nearby X-ray source, but also because it

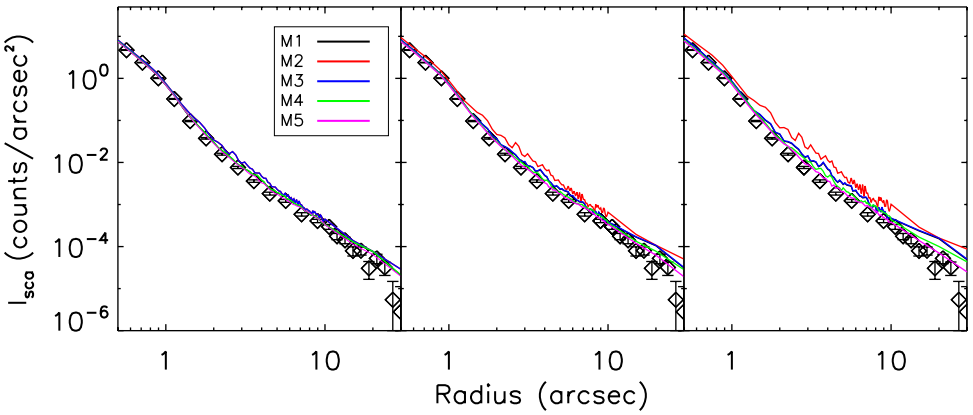

Figure 5.8: In this figure the panel shows the observation of AU Mic and five dust models with q=4.1 and SW50, $N_{\rm H} = 1 \times 10^{19}$ cm^{-2} and different dust mixtures. This panel corresponds with the lower left panel of Figure 5.7. The middle panel shows the same models, but now with $N_{\rm H} = 5 \times 10^{19}$ cm^{-2} and the right panel shows the models with $N_{\rm H} = 1 \times 10^{20}$ cm^{-2}.

has an edge-on configuration, which makes it in principle possible to observe the X-ray dust scattering. There exist more nearby debris disks, such as those of ϵ Eridani or Fomalhaut but these do not have an edge-on configuration. If the disk was slightly more face-on, the scattering angles involved become very large and the intensity of the scattered light drops precipitously. Other edge-on debris disks, such as the one of β Pictoris at a distance of 19.4 parsec or HD 139664 at a distance of 17.5 pc (Kalas et al., 2006), are situated too far away for current spatial resolution and are not as bright in the X-rays as AU Mic.

A moderately strong stellar wind model is favored in both the analysis of S15 and AB06. In our analysis, such a model provides the best conditions to observe the dust halo, since this model includes the smaller dust particles, that are the efficient scatterers.

The slope of the size distribution is an important parameter as well. For a flat distribution, the halo will not be prominent, since the small dust particles will be less prominently represented, which are the effective scatterers. Previous studies show that the value of the slope of the size distribution is still uncertain (AB06). S15 show a preference for a relatively shallow slope of 3.3, whereas Kalas et al. (2004) predict a steeper slope. The stellar wind may indeed also affect the size distribution of the grains since the smallest particles are more affected by transport than by collisions (S15). We also investigated the effect of the dust composition on the dust halo. As can be seen in Figure 5.7 the differences between the five different dust mixtures are at most one order of magnitude in the case of SW50. We also note that none of the dust models produce an observable dust signature in the halo.

Nevertheless, we can explore the parameter space slightly further. In Section 5.2 we determined the column density along the line of sight: 1×10^{19} cm^{-2}. This value is an upper limit, since the value of the vertical optical depth is at most $\tau = 5 \times 10^{-3}$ in the visible

(AB06). A direct measurement of the $N_{\rm H}$ was performed by Schneider and Schmitt (2010) using *Chandra* LETGS data obtaining a $N_{\rm H} < 1 \times 10^{19}$ cm^{-2}. The LETGS spectrum used in the analysis suffers from a high background contamination and the carbon edge used in the analysis contains a contribution from the carbon in the UV/Ion shield of the HRC-S detector. This introduces an uncertainty in the $N_{\rm H}$. From UV measurements a different upper limit of $N_{\rm H} < 5 \times 10^{19}$ cm^{-2} was obtained (France et al., 2007; Schneider and Schmitt, 2010). We increase the column density and explore at which value we may be able to observe the dust halo. In Figure 5.8 we show the results for the best case result from Figure 5.7 with the steepest slope (q=4.1) and moderate stellar wind strength (SW50), thus favoring the small particles. The first panel in Figure 5.8 shows the situation as in Figure 5.7. The second panel show the same models, but now with a $N_{\rm H}$ of 5×10^{19} cm^{-2} and the third panel show the models with a $N_{\rm H}$ of 1×10^{20} cm^{-2}. As can be seen in the second panel, most of the halo models, except for M5, begin to be visible. The effect is clearer in the third panel where all the models produce a visible dust halo above the PSF.

5.6 Conclusion

In this chapter, we explored a new parameter space in X-ray halo theory. We applied it to a realistic environment, where we use the system of AU Mic as a model. We find that models with a steeper slope, moderately strong stellar wind model and a composition of silicates and graphite are the ones that would enhance a theoretical halo. The models do not produce a significant scattering halo, using the current spatial resolution. Future X-ray missions may enable us to observe the X-ray halo of debris disks. Such a X-ray telescope would require a PSF which has a FWHM < 0.5 arcsec, i.e. smaller than the FWHM of *Chandra*. A possible future X-ray telescope called Lynx (also known as the X-ray Surveyor) may provide a more favorable angular resolution[4]. Such a PSF combined with an adequate effective area will make it possible to further explore the parameter space and in that way better constrain the dust size distribution and composition of the dust of the AU Mic debris disk system.

Acknowledgements

Dust studies at SRON and Leiden Observatory are supported through the Spinoza Premie of the Dutch science agency, NWO. We would like to thank Vinay Kashyap and Diab Jerius for their helpful suggestions concerning the data reduction. E.C. acknowledges support from NWO-Vidi grant 639.042.525.

[4]https://wwwastro.msfc.nasa.gov/lynx/

References

A'Hearn, M. F., Belton, M. J. S., Delamere, W. A., Kissel, J., Klaasen, K. P., McFadden, L. A., Meech, K. J., Melosh, H. J., Schultz, P. H., Sunshine, J. M., Thomas, P. C., Veverka, J., Yeomans, D. K., Baca, M. W., Busko, I., Crockett, C. J., Collins, S. M., Desnoyer, M., Eberhardy, C. A., Ernst, C. M., Farnham, T. L., Feaga, L., Groussin, O., Hampton, D., Ipatov, S. I., Li, J.-Y., Lindler, D., Lisse, C. M., Mastrodemos, N., Owen, W. M., Richardson, J. E., Wellnitz, D. D., and White, R. L. (2005). Deep Impact: Excavating Comet Tempel 1. *Science*, 310:258–264.

Augereau, J.-C. and Beust, H. (2006). On the AU Microscopii debris disk. Density profiles, grain properties, and dust dynamics. *A&A*, 455:987–999.

Backman, D. E. and Paresce, F. (1993). Main-sequence stars with circumstellar solid material - The VEGA phenomenon. In Levy, E. H. and Lunine, J. I., editors, *Protostars and Planets III*, pages 1253–1304.

Beardmore, A. P., Willingale, R., Kuulkers, E., Altamirano, D., Motta, S. E., Osborne, J. P., Page, K. L., and Sivakoff, G. R. (2016). Lord of the Rings - Return of the King: Swift-XRT observations of dust scattering rings around V404 Cygni. *MNRAS*, 462:1847–1863.

Beichman, C. A., Bryden, G., Gautier, T. N., Stapelfeldt, K. R., Werner, M. W., Misselt, K., Rieke, G., Stansberry, J., and Trilling, D. (2005). An Excess Due to Small Grains around the Nearby K0 V Star HD 69830: Asteroid or Cometary Debris? *ApJ*, 626:1061–1069.

Boccaletti, A., Thalmann, C., Lagrange, A.-M., Janson, M., Augereau, J.-C., Schneider, G., Milli, J., Grady, C., Debes, J., Langlois, M., Mouillet, D., Henning, T., Dominik, C., Maire, A.-L., Beuzit, J.-L., Carson, J., Dohlen, K., Engler, N., Feldt, M., Fusco, T., Ginski, C., Girard, J. H., Hines, D., Kasper, M., Mawet, D., Ménard, F., Meyer, M. R., Moutou, C., Olofsson, J., Rodigas, T., Sauvage, J.-F., Schlieder, J., Schmid, H. M., Turatto, M., Udry, S., Vakili, F., Vigan, A., Wahhaj, Z., and Wisniewski, J. (2015). Fast-moving features in the debris disk around AU Microscopii. *Nature* , 526:230–232.

Bruggeman, D. A. G. (1935). Berechnung verschiedener physikalischer Konstanten von heterogenen Substanzen. I. Dielektrizitätskonstanten und Leitfähigkeiten der Mischkörper aus isotropen Substanzen. *Annalen der Physik*, 416:636–664.

Burns, J. A., Lamy, P. L., and Soter, S. (1979). Radiation forces on small particles in the solar system. *Icarus*, 40:1–48.

Carter, C., Karovska, M., Jerius, D., Glotfelty, K., and Beikman, S. (2003). ChaRT: The Chandra Ray Tracer. In Payne, H. E., Jedrzejewski, R. I., and Hook, R. N., editors, *Astronomical Data Analysis Software and Systems XII*, volume 295 of *Astronomical Society of the Pacific Conference Series*, page 477.

Chen, C. H., Fitzgerald, M. P., and Smith, P. S. (2008). A Possible Icy Kuiper Belt around HD 181327. *ApJ*, 689:539–544.

Costantini, E., Freyberg, M. J., and Predehl, P. (2005). Absorption and scattering by interstellar dust: an XMM-Newton observation of <ASTROBJ>Cyg X-2</ASTROBJ>. *A&A*, 444:187–200.

Cully, S. L., Siegmund, O. H. W., Vedder, P. W., and Vallerga, J. V. (1993). Extreme Ultraviolet Explorer deep survey observations of a large flare on AU Microscopii. *ApJ*, 414:L49–L52.

de Vries, B. L., Acke, B., Blommaert, J. A. D. L., Waelkens, C., Waters, L. B. F. M., Vandenbussche, B., Min, M., Olofsson, G., Dominik, C., Decin, L., Barlow, M. J., Brandeker, A., di Francesco, J., Glauser, A. M., Greaves, J., Harvey, P. M., Holland, W. S., Ivison, R. J., Liseau, R., Pantin, E. E., Pilbratt, G. L., Royer, P., and Sibthorpe, B. (2012). Comet-like mineralogy of olivine crystals in an extrasolar proto-Kuiper belt. *Nature* , 490:74–76.

Dohnanyi, J. S. (1969). Collisional Model of Asteroids and Their Debris. *J. Geophys. Res.*, 74:2531–2554.

Draine, B. T. (2003). Scattering by Interstellar Dust Grains. II. X-Rays. *ApJ*, 598:1026–1037.

Draine, B. T. and Lee, H. M. (1984). Optical properties of interstellar graphite and silicate grains. *ApJ*, 285:89–108.

Durda, D. D. and Dermott, S. F. (1997). The Collisional Evolution of the Asteroid Belt and Its Contribution to the Zodiacal Cloud. *Icarus*, 130:140–164.

Fitzgerald, M. P., Kalas, P. G., Duchêne, G., Pinte, C., and Graham, J. R. (2007). The AU Microscopii Debris Disk: Multiwavelength Imaging and Modeling. *ApJ*, 670:536–556.

France, K., Roberge, A., Lupu, R. E., Redfield, S., and Feldman, P. D. (2007). A Low-Mass H_2 Component to the AU Microscopii Circumstellar Disk. *ApJ*, 668:1174–1181.

Gallagher, D., Cash, W., and Green, J. (1995). A search for an X-ray scattering halo around Scorpius X-1. *ApJ*, 439:976–982.

Graham, J. R., Kalas, P. G., and Matthews, B. C. (2007). The Signature of Primordial Grain Growth in the Polarized Light of the AU Microscopii Debris Disk. *ApJ*, 654:595–605.

Hawley, S. L., Gizis, J. E., and Reid, I. N. (1996). The Palomar/MSU Nearby Star Spectroscopic Survey.II.The Southern M Dwarfs and Investigation of Magnetic Activity. *AJ*, 112:2799.

Hayakawa, S. (1973). Cosmic X-Rays and Interstellar Dust. In Greenberg, J. M. and van de Hulst, H. C., editors, *Interstellar Dust and Related Topics*, volume 52 of *IAU Symposium*, page 283.

Heinz, S., Burton, M., Braiding, C., Brandt, W. N., Jonker, P. G., Sell, P., Fender, R. P., Nowak, M. A., and Schulz, N. S. (2015). Lord of the Rings: A Kinematic Distance to Circinus X-1 from a Giant X-Ray Light Echo. *ApJ*, 806:265.

Henke, B. L., Gullikson, E. M., and Davis, J. C. (1993). X-Ray Interactions: Photoabsorption, Scattering, Transmission, and Reflection at E = 50-30,000 eV, Z = 1-92. *Atomic Data and Nuclear Data Tables*, 54:181–342.

Hoffman, J. and Draine, B. T. (2016). Accurate Modeling of X-ray Extinction by Interstellar Grains. *ApJ*, 817:139.

Kalas, P., Graham, J. R., Clampin, M. C., and Fitzgerald, M. P. (2006). First Scattered Light Images of Debris Disks around HD 53143 and HD 139664. *ApJ*, 637:L57–L60.

Kalas, P., Liu, M. C., and Matthews, B. C. (2004). Discovery of a Large Dust Disk Around the Nearby Star AU Microscopii. *Science*, 303:1990–1992.

Krist, J. E., Stapelfeldt, K. R., Golimowski, D. A., Ardila, D. R., Clampin, M., Martel, A. R., Ford, H. C., Illingworth, G. D., and Hartig, G. F. (2005). Hubble Space Telescope ACS Images of the GG Tauri Circumbinary Disk. *AJ*, 130:2778–2787.

Krivov, A. V. (2010). Debris disks: seeing dust, thinking of planetesimals and planets. *Research in Astronomy and Astrophysics*, 10:383–414.

Lagrange, A.-M., Backman, D. E., and Artymowicz, P. (2000). Planetary Material around Main-Sequence Stars. *Protostars and Planets IV*, page 639.

Laor, A. and Draine, B. T. (1993). Spectroscopic constraints on the properties of dust in active galactic nuclei. *ApJ*, 402:441–468.

Lebreton, J., Augereau, J.-C., Thi, W.-F., Roberge, A., Donaldson, J., Schneider, G., Maddison, S. T., Ménard, F., Riviere-Marichalar, P., Mathews, G. S., Kamp, I., Pinte, C., Dent, W. R. F., Barrado, D., Duchêne, G., Gonzalez, J.-F., Grady, C. A., Meeus, G., Pantin, E., Williams, J. P., and Woitke, P. (2012). An icy Kuiper belt around the young solar-type star HD 181327. *A&A*, 539:A17.

Lebreton, J., van Lieshout, R., Augereau, J.-C., Absil, O., Mennesson, B., Kama, M., Dominik, C., Bonsor, A., Vandeportal, J., Beust, H., Defrère, D., Ertel, S., Faramaz, V., Hinz, P., Kral, Q., Lagrange, A.-M., Liu, W., and Thébault, P. (2013). An interferometric study of the Fomalhaut inner debris disk. III. Detailed models of the exozodiacal disk and its origin. *A&A*, 555:A146.

Lisse, C. M., Beichman, C. A., Bryden, G., and Wyatt, M. C. (2007). On the Nature of the Dust in the Debris Disk around HD 69830. *ApJ*, 658:584–592.

Lisse, C. M., Chen, C. H., Wyatt, M. C., Morlok, A., Song, I., Bryden, G., and Sheehan, P. (2009). Abundant Circumstellar Silica Dust and SiO Gas Created by a Giant Hypervelocity Collision in the ~12 Myr HD172555 System. *ApJ*, 701:2019–2032.

MacGregor, M. A., Wilner, D. J., Rosenfeld, K. A., Andrews, S. M., Matthews, B., Hughes, A. M., Booth, M., Chiang, E., Graham, J. R., Kalas, P., Kennedy, G., and Sibthorpe, B. (2013). Millimeter Emission Structure in the First ALMA Image of the AU Mic Debris Disk. *ApJ*, 762:L21.

Magee, H. R. M., Güdel, M., Audard, M., and Mewe, R. (2003). An XMM-Newton observation of the flare star AU MIC. *Advances in Space Research*, 32:1149–1154.

Mamajek, E. E. and Bell, C. P. M. (2014). On the age of the β Pictoris moving group. *MNRAS*, 445:2169–2180.

Martin, P. G. (1970). On the interaction of cosmic X-rays with interstellar grains. *MNRAS*, 149:221.

Mathis, J. S. and Lee, C.-W. (1991). X-ray halos as diagnostics of interstellar grains. *ApJ*, 376:490–499.

Mathis, J. S., Rumpl, W., and Nordsieck, K. H. (1977). The size distribution of interstellar grains. *ApJ*, 217:425–433.

Mauche, C. W. and Gorenstein, P. (1986). Measurements of X-ray scattering from interstellar grains. *ApJ*, 302:371–387.

Metchev, S. A., Eisner, J. A., Hillenbrand, L. A., and Wolf, S. (2005). Adaptive Optics Imaging of the AU Microscopii Circumstellar Disk: Evidence for Dynamical Evolution. *ApJ*, 622:451–462.

Mitra-Kraev, U., Harra, L. K., Güdel, M., Audard, M., Branduardi-Raymont, G., Kay, H. R. M., Mewe, R., Raassen, A. J. J., and van Driel-Gesztelyi, L. (2005). Relationship between X-ray and ultraviolet emission of flares from dMe stars observed by XMM-Newton. *A&A*, 431:679–686.

Monsignori Fossi, B. C., Landini, M., Del Zanna, G., and Bowyer, S. (1996). A Time-resolved Extreme-Ultraviolet Spectroscopic Study of the Quiescent and Flaring Corona of the Flare Star AU Microscopii. *ApJ*, 466:427.

Murray, S. S., Chappell, J. H., Kenter, A. T., Juda, M., Kraft, R. P., Zombeck, M. V., Meehan, G. R., Austin, G. K., and Gomes, J. J. (2000). Event screening for the Chandra X-Ray Observatory High-Resolution Camera (HRC). In Flanagan, K. A. and Siegmund, O. H., editors, *X-Ray and Gamma-Ray Instrumentation for Astronomy XI*, volume 4140 of *Proc. SPIE*, pages 144–154.

Overbeck, J. W. (1965). Small-Angle Scattering of Celestial X-Rays by Interstellar Grains. *ApJ*, 141:864.

Perryman, M. A. C., Lindegren, L., Kovalevsky, J., Hoeg, E., Bastian, U., Bernacca, P. L., Crézé, M., Donati, F., Grenon, M., Grewing, M., van Leeuwen, F., van der Marel, H., Mignard, F., Murray, C. A., Le Poole, R. S., Schrijver, H., Turon, C., Arenou, F., Froeschlé, M., and Petersen, C. S. (1997). The HIPPARCOS Catalogue. *A&A*, 323:L49–L52.

Predehl, P. and Schmitt, J. H. M. M. (1995). X-raying the interstellar medium: ROSAT observations of dust scattering halos. *A&A*, 293:889–905.

Robinson, R. D., Linsky, J. L., Woodgate, B. E., and Timothy, J. G. (2001). Far-Ultraviolet Observations of Flares on the dM0e Star AU Microscopii. *ApJ*, 554:368–382.

Sanz-Forcada, J., Brickhouse, N. S., and Dupree, A. K. (2003). The Structure of Stellar Coronae in Active Binary Systems. *ApJS*, 145:147–179.

Schneider, P. C. and Schmitt, J. H. M. M. (2010). X-raying the AU Microscopii debris disk. *A&A*, 516:A8.

Schüppler, C., Löhne, T., Krivov, A. V., Ertel, S., Marshall, J. P., Wolf, S., Wyatt, M. C., Augereau, J.-C., and Metchev, S. A. (2015). Collisional modelling of the AU Microscopii debris disc. *A&A*, 581:A97.

Smith, R. K., Dame, T. M., Costantini, E., and Predehl, P. (2006). The X-Ray Halo of GX 5-1. *ApJ*, 648:452–460.

Smith, R. K. and Dwek, E. (1998). Soft X-Ray Scattering and Halos from Dust. *ApJ*, 503:831–842.

Smith, R. K., Valencic, L. A., and Corrales, L. (2016). The Impact of Accurate Extinction Measurements for X-Ray Spectral Models. *ApJ*, 818:143.

Song, I., Weinberger, A. J., Becklin, E. E., Zuckerman, B., and Chen, C. (2002). M-Type Vega-like Stars. *AJ*, 124:514–518.

Song, I., Zuckerman, B., Weinberger, A. J., and Becklin, E. E. (2005). Extreme collisions between planetesimals as the origin of warm dust around a Sun-like star. *Nature* , 436:363–365.

Strubbe, L. E. and Chiang, E. I. (2006). Dust Dynamics, Surface Brightness Profiles, and Thermal Spectra of Debris Disks: The Case of AU Microscopii. *ApJ*, 648:652–665.

Su, K. Y. L., Rieke, G. H., Misselt, K. A., Stansberry, J. A., Moro-Martin, A., Stapelfeldt, K. R., Werner, M. W., Trilling, D. E., Bendo, G. J., Gordon, K. D., Hines, D. C., Wyatt, M. C., Holland, W. S., Marengo, M., Megeath, S. T., and Fazio, G. G. (2005). The Vega Debris Disk: A Surprise from Spitzer. *ApJ*, 628:487–500.

Tan, J. C. and Draine, B. T. (2004). X-Ray Scattering Halos from the Galactic Center: Implications for Diffuse Emission around Sagittarius A*. *ApJ*, 606:296–305.

Tiengo, A., Vianello, G., Esposito, P., Mereghetti, S., Giuliani, A., Costantini, E., Israel, G. L., Stella, L., Turolla, R., Zane, S., Rea, N., Götz, D., Bernardini, F., Moretti, A., Romano, P., Ehle, M., and Gehrels, N. (2010). The Dust-scattering X-ray Rings of the Anomalous X-ray Pulsar 1E 1547.0-5408. *ApJ*, 710:227–235.

Tsikoudi, V. (1988). Flare stars detected by the Infrared Astronomical Satellite. *AJ*, 95:1797–1800.

Valencic, L. A. and Smith, R. K. (2015). Interstellar Dust Properties from a Survey of X-Ray Halos. *ApJ*, 809:66.

van Leeuwen, F. (2007). Validation of the new Hipparcos reduction. *A&A*, 474:653–664.

Vasilopoulos, G. and Petropoulou, M. (2016). The X-ray dust-scattered rings of the black hole low-mass binary V404 Cyg. *MNRAS*, 455:4426–4441.

Vaughan, S., Willingale, R., O'Brien, P. T., Osborne, J. P., Reeves, J. N., Levan, A. J., Watson, M. G., Tedds, J. A., Watson, D., Santos-Lleó, M., Rodríguez-Pascual, P. M., and Schartel, N. (2004). The Discovery of an Evolving Dust-scattered X-Ray Halo around GRB 031203. *ApJ*, 603:L5–L8.

Wiener, O. (1910). Zur Theorie der Refraktionskonstanten. *Berichte über die Verhandlungen der Königlich-Sächsischen Gesellschaft der Wisseschaften zu Leipzig, Math.-phys. Klasse*, 62:256–277.

Wood, B. E., Redfield, S., Linsky, J. L., Müller, H.-R., and Zank, G. P. (2005). Stellar Lyα Emission Lines in the Hubble Space Telescope Archive: Intrinsic Line Fluxes and Absorption from the Heliosphere and Astrospheres. *ApJS*, 159:118–140.

Wyatt, M. C. (2005). The insignificance of P-R drag in detectable extrasolar planetesimal belts. *A&A*, 433:1007–1012.

Wyatt, M. C. (2008). Evolution of Debris Disks. *ARA&A*, 46:339–383.

Wyatt, M. C. and Dent, W. R. F. (2002). Collisional processes in extrasolar planetesimal discs - dust clumps in Fomalhaut's debris disc. *MNRAS*, 334:589–607.